



Microfossil and geochemical evidence for the Storegga tsunami at Budle Bay, Northumberland, UK

Leeza O. Pickering^{1*} , Grace F. Summers^{1,2} , Emma P. Hocking¹ , Ed Garrett³ , Alexander R. Simms⁴ 

¹ Department of Geography and Environmental Sciences, Northumbria University, Newcastle-upon-Tyne, NE1 8ST, UK

² Department of Geography, Durham University, Durham, DH1 3LE, UK

³ Department of Environment and Geography, University of York, York, YO10 5NG, UK

⁴ Department of Earth Science, University of California Santa Barbara, Santa Barbara, CA 93106, USA

*corresponding author: Leeza O. Pickering (leeza.o.pickering@northumbria.ac.uk)

doi: [10.57035/journals/sdk.2024.e22.1280](https://doi.org/10.57035/journals/sdk.2024.e22.1280)

Editors: Ian Kane and Latisha Brengman

Reviewers: Two anonymous reviewers

Copyediting, layout and production: Romain Vaucher and Thomas J. H. Dodd

Submitted: 10.10.2023

Accepted: 02.07.2024

Published: 12.08.2024

Abstract | Evidence for the Storegga tsunami, which was generated by one of the world's largest submarine slides, is well documented in Scotland, but the southerly extent of tsunami inundation in the UK is far more uncertain. Here, we combine new sedimentological, geochemical, microfossil, and ground-penetrating radar datasets to investigate the origins of two sand beds at Budle Bay, Northumberland. The lower of these two sand deposits is a fine- to medium-grained sand that fines upwards, is dominated by fragmented marine diatom taxa, and is characterised by elevated calcium concentrations. Two radiocarbon dated samples provide minimum age constraints on the timing of the deposition of the lower sand at around 8120–8380 cal yr BP. It is tentatively interpreted as being deposited by the Storegga tsunami. The upper sand bed is generally finer grained than the lower sand, and the calcium concentrations are considerably lower. One hypothesis is that the upper sand was deposited by the 1953 CE storm surge, but additional chronological control is required to test this interpretation. Our findings highlight the challenges associated with differentiating between storm and tsunami deposits and confirm the localised nature of preservation of Storegga tsunami deposits.

Lay summary | Evidence shows that the Storegga tsunami, caused by one of the world's largest underwater landslides, reached many parts of eastern Scotland. However, further south, it's far more uncertain where this tsunami impacted. Here, we investigated sediments at Budle Bay in Northumberland, including the sediment type, their chemistry and the small fossils they contain, which in combination can provide clues about the type of conditions the sediments were deposited in, and their source. We used this information to determine the origins of two layers of sand at Budle Bay. The oldest of these sand layers was deposited between 8380 and 8120 years ago, which fits with when we know the Storegga tsunami occurred. It consists mainly of marine debris and has a high calcium content, suggesting it may have been left by the Storegga tsunami. The upper sand layer is finer-grained and has less calcium. The upper sand was possibly deposited by a storm surge in 1953, although more evidence is needed to confirm this. Our study highlights the difficulty in finding the difference between deposits left by storms and tsunamis, and how locally the impact of the Storegga tsunami can be preserved.

Keywords: Tsunami, Storm deposits, Geochemistry, Diatoms, Doggerland

1. Introduction

Regarded as one of the world's largest submarine landslides, the Storegga slide occurred on the continental slope west of Norway (Figure 1A) around 8080–8180 cal yr BP (Bondevik et al., 2012; Rush et al., 2023). The slide produced a tsunami that reached onshore elevations of

10–12 m in western Norway, 20 m on the Shetland Islands, 3–9 m in northwest Scotland, and 3–6 m in northeast Scotland (Bondevik et al., 2005; Woodroffe et al., 2023). Model simulations suggest that a magnitude 6.5–7.0 earthquake was a possible trigger of the slope failure within the Storegga region (Leynaud et al., 2009), destabilizing 2,400–3,200 km³ of sediment and affecting an area of

~95,000 km² (Haflidason et al., 2005; Tappin, 2017). Seismic data suggest the Storegga slide was a deforming translational landslide rather than a slump, with slope failure at a water depth of 1000 m, rather than at the top of the slope as suggested by theoretical models (Tappin, 2017). The large-scale sliding occurred as a response to the cyclic nature of sedimentation from climatic oscillations at the end of, or soon after, glaciation in three discrete events, with the second event generating the tsunami (Micallef et al., 2009).

Storegga tsunami deposits have been observed in coastal areas of Scotland (Dawson et al., 1988; Dawson & Smith, 2000; Smith et al., 2004; Long et al., 2016; Rush et al., 2023; Woodroffe et al., 2023), the Shetland and Faroe Islands (Grauert et al., 2001; Bondevik et al., 2003), Greenland (Wagner et al., 2007), Norway (Bondevik et al., 1997), and Denmark (Fruegaard et al., 2015). Storegga tsunami deposits identified in the UK are generally described as fine- to medium-grained sands that are up to 30 cm thick, and contain one or more fining upwards sequences (Dawson et al., 1988; Dawson & Smith, 2000; Smith et al., 2004). Deposits in sheltered or inland areas are typically characterised by a single fining upwards sequence, and those from more exposed seaward locations often feature two or more fining upwards sequences (Smith et al., 2004). Storegga deposits often contain fragments of organic material, silt, and rip-up clasts composed of peat (Smith et al., 2004). In terms of microfossil content, Storegga deposits are generally dominated by both marine and brackish taxa (notably the diatom species *Paralia sulcata* and *Cocconeis scutellum*), and high percentages of broken diatom valves (Dawson et al., 1988; Dawson & Smith, 2000; Smith et al., 2004).

In the UK, whilst Storegga deposits are well reported and described in Scotland, evidence of the southerly extent of tsunami inundation is far more uncertain and limited to several possible sites in northern England (Shennan et al., 2000; Boomer et al., 2007), as well as an offshore site in the southern North Sea (Gaffney et al., 2020). Along the Northumberland coastline, coarse-grained sand beds observed at Broomhouse Farm (Shennan et al., 2000) and Howick (Boomer et al., 2007), which are preserved within otherwise fine-grained sediment sequences, were proposed as possible Storegga tsunami deposits, but alternative depositional mechanisms for these deposits, such as storms, fluvial transport, or mass movements, could not be ruled out (Sharrocks & Hill, 2023). At Annstead Burn, a similar coarse-grained sand bed was identified, but overlying deposits were dated to a few centuries older than the Storegga tsunami (Shennan et al., 2000). Therefore, it is currently inconclusive whether the Storegga tsunami is recorded on the Northumberland coastline.

In this study, we aim to address these debates and seek evidence of the Storegga tsunami along the Northumberland coastline by using geochemical and microfossil evidence to help distinguish between storm and tsunami deposits,

and radiocarbon dating to recognise deposits of the appropriate age to identify the event. We intend this study as a contribution to the growing body of literature aimed at distinguishing tsunami and storm deposits that recognise the considerable challenges associated with identifying ancient tsunami deposits (Kortekaas & Dawson, 2007; Morton et al., 2007; Engel & Brückner, 2011; Engel et al., 2020; Gaffney et al., 2020).

2. Study site

The study is based at Budle Bay, which is located on the north Northumberland coast between Bamburgh ~2.5 km to the southeast and Holy Island ~6 km to the north (Figure 1). Budle Bay occupies an area of 276 ha and is a square-shaped inlet ~1.6 km wide, opening to the North Sea along its northeastern side. The intertidal zone is extensive, and the estuary is macrotidal, with a tidal range of 4.2 m (Davidson & Buck, 1997). Two small rivers flow into Budle Bay, Waren Burn in the south and the smaller Ross Low in the northwest, with the two streams coalescing in the intertidal zone to form the Budle Water that flows north-eastward. The underlying geology of the area is dominated by limestones of the Alston Formation, which are overlain by superficial alluvium deposits (British Geological Survey, 2020). Extensive sand dunes form Ross Links to the north, and sand spits line the entrance to the bay both to the north and south. Dating of aeolian sediments from Ross Links suggests primary dune building occurred during the Little Ice Age as a result of major storm activity (Wilson et al., 2001). The absence of dune systems prior to this is the result of the coastal configuration, shoreline regression, and sediment availability (Wilson et al., 2001). Budle Bay was the site of a seaport between 1240 CE and the early twentieth century, and maps from the mid-19th century show the presence of a pier within the otherwise natural harbour of Budle Bay, which was probably used for grain export (Linsley, 2005). Today the bay forms part of the Lindisfarne National Nature Reserve. Flood defences in the form of an embankment are situated on the northeast shore of Budle Bay and a sluice gate at Ross Low (Figure 1C; Guthrie et al., 2009; Environment Agency National Flood and Coastal Defence Database). Notable flooding on the north shore of Budle Bay, on the Ross Peninsula, occurred in August 1948 and on 30th January 1953, the latter requiring the repair and rebuilding of flood defences (Guthrie et al., 2009).

In terms of relative sea-level history, the site lies around the transition between Holocene emergence to the north and submergence to the south. Twenty sea-level index points from six nearby sites record relative sea-level rise between 9 and 2.5 ka BP from ~5 m below present, reaching a mid-late Holocene highstand ~2.5 m above present (Shennan et al., 2000). The age of this maximum is poorly constrained, but there is evidence for a relatively stable period of sea level in north Northumberland within a 1 m range, 1.5–2.5 m above present, between 7.2 and 3.6 ka BP (Shennan et al., 2000).

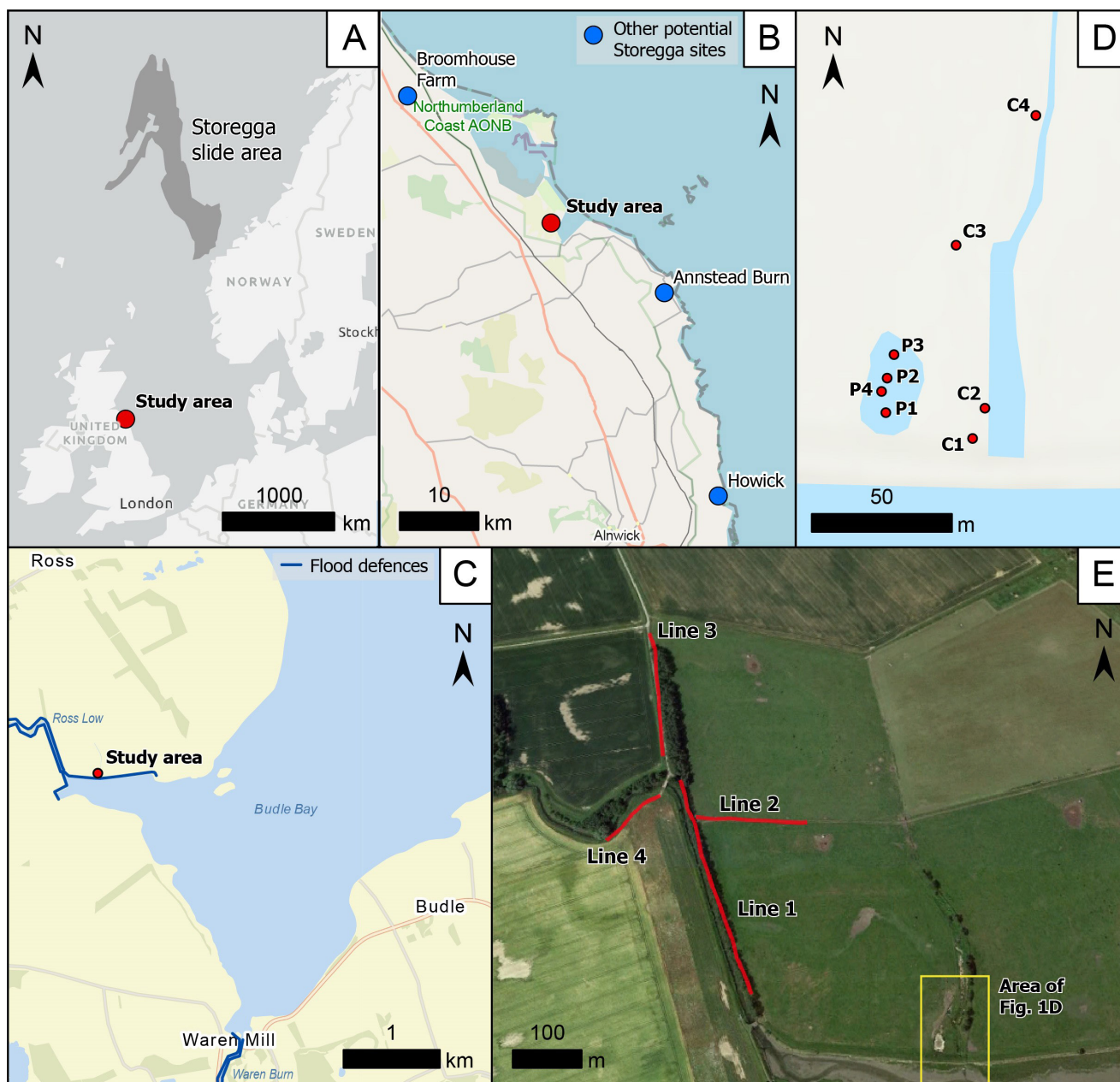


Figure 1 | Study area and core locations on the northeast coast of Northumberland, UK. Study area is shown relative to (A) the Storegga slide; (B) nearby Northumberland coastal sites; and (C) Budle Bay. (D) Core locations within a relict channel (C1–4) and pond (P1–4), and (E) ground-penetrating radar lines (red). Figures 1A–D created with the Esri ArcGIS software; Figure 1E: ©Google Earth, Landsat/Copernicus image taken on 7 January 2018.

3. Material and methods

Eight sediment cores were collected from a relict channel of the estuary at Ross Low on the northern coast of Budle Bay (Figure 1D). Cores C1–C4 and P1–3 were collected in 2018 using a 2.5 cm diameter gouge corer, and core P4 was collected in 2020 with a 5 cm diameter Russian corer. Core locations and elevations were obtained using a Leica differential GPS, with a vertical accuracy of ± 6 mm. Core top locations range in elevation between 2.93 and 3.42 m OD (Figure 2). Lithology was described in the field using the Troels-Smith (1955) classification scheme (Supplemental material). Cores P2, P3, P4 were preserved for particle size, geochemical and diatom analysis, and radiocarbon dating. Subsurface deposits in the field area were mapped using ground-penetrating radar.

Representative particle size for the study site was measured on core P2 at intervals of 1–2.5 cm throughout the core, which was dependent upon material availability and proximity to contacts between sediment units. All sub-samples were first treated with 20% hydrogen peroxide digest to remove all organic fractions. Particle size was measured using a Malvern Mastersizer 2000.

Quantitative geochemical analysis of cores P2, P3 and P4 was completed using energy-dispersive X-ray fluorescence (EDXRF). A total of 34 pellet samples were prepared across the three cores. As P2 and P3 were narrow gouge cores, broader sampling intervals were required than for core P4 to ensure a minimum wet weight (~ 4 g) to make pellet samples. Samples were dried in a drying cupboard and then ground into a fine powder using a pestle and mortar. Samples were then combined with a binding agent

(Cerox) using the RETSCH MM 200 mortar grinder for 45 seconds (frequency 25 Hz). Mixed samples were manually pressed into a cylinder die and individually run through a calibrated portable SPECTROSCOUT ED-XRF scanner.

Sub-samples for diatom analysis were taken at 0.5 cm intervals from core P4, and at 1–2.5 cm intervals from cores P2 and P3, depending on material available and proximity to contacts between sediment units. Diatom samples were prepared following standard procedures (Battarbee, 1986; Battarbee et al., 2001). A minimum of 250 valves were counted per sample. Diatom identification followed Hartley (1996) and Jüttner et al. (2023).

Three radiocarbon samples were analysed at the Belfast CHRONO Centre; two samples from core P2 (shell and wood) and one sample from core P3 (wood). The ages of wood samples were calibrated in OxCal 4.4 (Bronk Ramsey, 2009) using the terrestrial calibration curve, IntCal20 (Reimer et al., 2020). The shell date was calibrated using the Marine20 calibration curve (Heaton et al., 2020). No local offset (ΔR) was applied due to stable and negligible ΔR values reported from this region (Russell et al., 2015).

In addition to the analyses that were completed on the cores, four ground-penetrating radar (GPR) profiles were

collected to the north and west of the core sites (Figure 1E) to determine if the sand layers could be imaged. GPR lines were collected using a Mala Geosystems RAMAC GPR, with an unshielded 200 MHz antennae that was pulled on a Durham University custom sled equipped with an antenna separation of 50 cm. Unfortunately, high-resolution GPS data were not available for a topographical correction, thus data were only collected across the well-graded flat roads, which lacked significant topographical relief (~<50 cm over ~250 m). Processing was limited to simple manually-applied depth gain, stacking, and band-pass filtering.

4. Results

4.1. Lithostratigraphy and particle size analysis

Of the eight cores evaluated for this study, four cores (P1–4) were recovered from what is interpreted as a desiccated pond within a palaeochannel, while the remaining four cores (C1–4) likely contain sediments deposited within a palaeochannel (Figure 1D). Three cores (P1, P2, and P3), all from the pond location and within 30 m of the shoreline, captured a sand unit below an elevation of 1 m OD, which we interpreted as a candidate deposit of the Storegga tsunami (Figure 2). The lower stratigraphy in these three

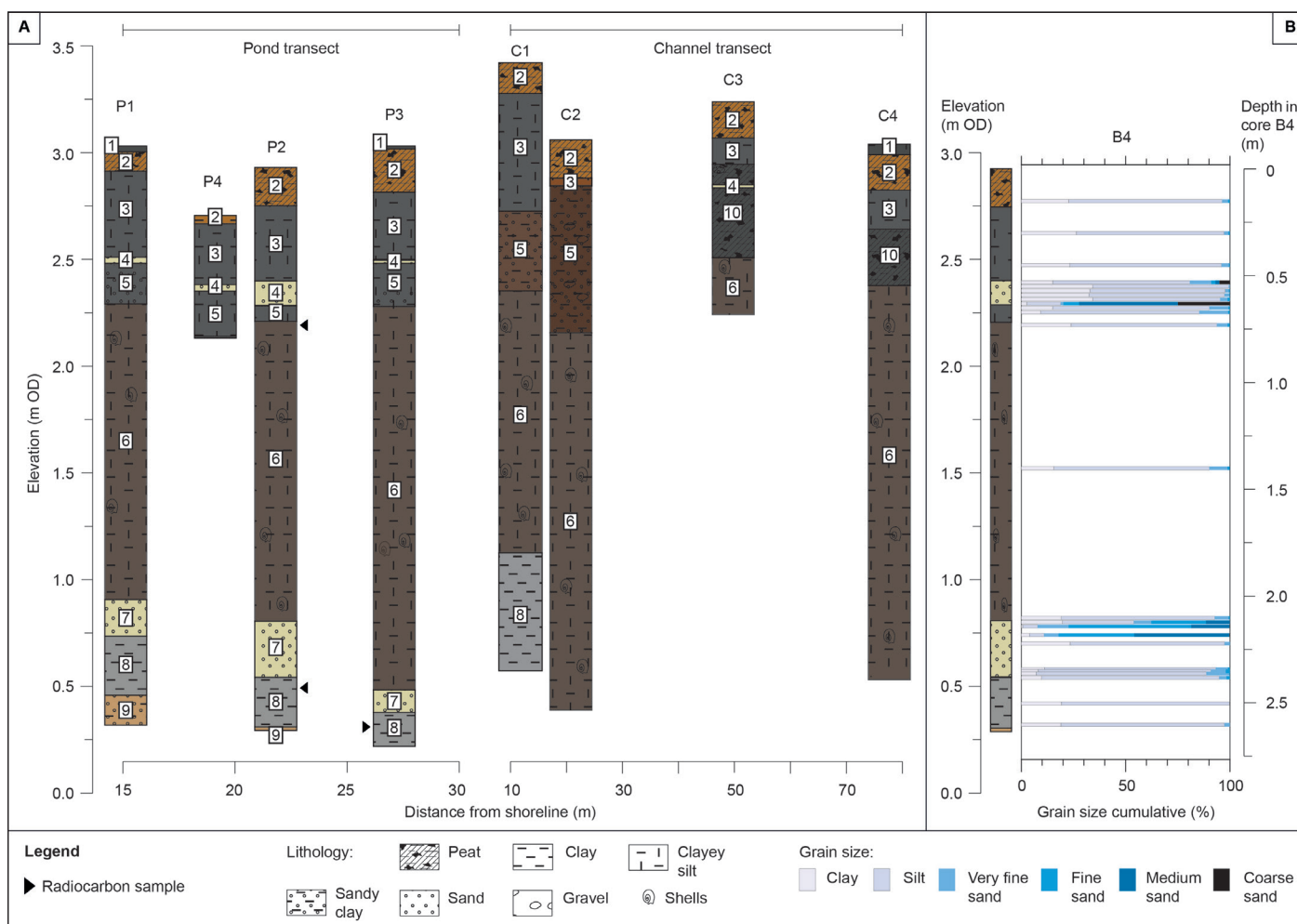


Figure 2 | (A) Lithostratigraphy of cores recovered from Budle Bay, Northumberland; (B) Particle size analysis from core P2. For full sediment descriptions and Troels-Smith classification, see Supplementary Table 1. Colours of sedimentary units broadly reflect sediment colour.

cores consists of consolidated grey clay (unit 8), which is abruptly overlain by a grey fine- to medium-grained sand that is 8–24 cm thick (unit 7, hereafter referred to as the 'lower sand') (Figure 2A; Supplementary Table 1). The elevation of the lower sand is 0.74–0.91 m OD, 0.57–0.81 m OD, and 0.38–0.46 m OD in cores P1, P2, and P3, respectively. Particle size analysis for core P2 indicates the sands fine upwards (Figure 2B). The sand is abruptly overlain by over a metre of brown-grey silty clay that contains abundant shell material (unit 6 in Figure 2A). The top of this shelly unit is ~2.2–2.3 m OD. Capping unit 6 is unit 5, a dark brown-grey silty clay with sand lenses and sharp upper and lower contacts. A medium- to coarse-grained grey sand that is 1–9 cm thick (unit 4, hereafter referred to as the 'upper sand') overlies unit 5, again with sharp upper and lower contacts. The elevation of the bottom of the upper sand ranges between 2.29–2.50 m OD. Particle size analysis shows the upper sand fines upwards from a medium- to coarse-grained sand (52% medium-grained, 25% coarse-grained sand in basal sample of the 'upper sand') into a sandy silt (maximum 19% sand in other 'upper sand' samples) (Figure 2B). An upper sand is also preserved in core P4 at 2.4 m OD, also within the pond location. The uppermost stratigraphy of cores P1–4 consists of grey-black organic clayey silt overlain by orange-brown organic clayey silt (units 1 and 2 in Figure 2A). A 1 cm-thick sand bed is observed in core C3, ~50 m inland from the shoreline (Figure 1D; unit 4 in Figure 2A), at a similar depth to the depth of the upper sand in the pond cores (2.8 m OD), but no other sand beds are observed in the remaining three cores from the palaeochannel.

4.2. Geochemical analysis

The geochemical signatures of the upper and lower sands are comparable (Figure 3) in cores P2 and P4, and in P2 and P3, respectively, in that they both show lower concentrations of terrestrial (Zr and Ti) and fine-grained indicators (K and Rb) relative to the sediments above and below (Figure 3A, B). Si profiles are also similar across both sands, with greater variability throughout the sand compared to muds and peats. However, the upper and lower sand beds differ in Ca concentrations. The lower sand in P2 and P3 shows higher Ca concentrations and higher Ca/Ti ratios than compared with the upper sand, and higher values relative to the underlying sediments (Figure 3). Ca concentrations also decrease throughout the upper sand, correlating with Br, another marine-sourced element. Ca concentrations do not decrease through the lower sand.

4.3. Diatom analysis

A total of 164 different diatom species were identified across 40 samples from cores P2, P3 and P4 (Figure 4). A minimum of 250 valves were counted per sample, with the exception of samples where the sediment was coarse-grained and diatoms were sparse. There were no diatoms present in the clay (unit 8) underlying the lower sand in both cores P2 and P3 (Figure 4A, C).

From the counts obtained, the lower sand in both P2 and P3 is dominated by a single taxon, *Paralia sulcata* (57–98%) (Figure 4A, C). There are small, but notable occurrences of freshwater and brackish taxa, most notably *Diploneis didyma* in P3 (up to 12%). It is impossible to comment on assemblage changes pre- and post-deposition of the lower sand due to a lack of diatom preservation in pre-sand clays. Diatom preservation (or abundances) are also very low in sediments deposited above the sand, making it hard to draw robust conclusions. However, it does appear that *Paralia sulcata* similarly dominates both the lower sand and the clays above.

By contrast, the upper sand is composed of a mixed diatom assemblage of marine, brackish, and freshwater species (Figure 4A, B). We note, however, that diatom preservation issues make comparison of the upper and lower sands on the basis of diatom assemblages challenging. The upper sand in both cores P2 and P4 is dominated by *Paralia sulcata*, *Planothidium delicatulum*, and *Tabularia fasciculata*. In P2, *Pseudostaurosira brevistriata*, *Pseudostaurosira elliptica*, and *Tryblionella apiculata* also dominate the upper sand, along with *Opephora mutabilis*, *Caloneis westii*, *Cyclotella meneghiniana*, and *Tryblionella acuminata* in P4.

In core P4, the diatom assemblage of the upper sand bed is not distinctly different to the assemblage of the clays deposited before and after, with *Paralia sulcata* and *Opephora mutabilis* being the dominant taxa in both (Figure 4B). In P2, whilst there are no taxa unique to the sand, the relative abundance of taxa differs between the sands and surrounding clays, and diatom assemblages also change pre- and post-sand deposition (Figure 4A). *Fallacia pygmaea* and *Tabularia fasciculata* occur prior to upper sand deposition, but not after. By contrast, *Staurosira construens* var. *venter* and *Navicula peregrina* increase in abundance post-sand deposition.

4.4. Chronology

Two wood samples, taken from just below the lower sand units in P2 and P3 (Figure 2A), date to 8208–8518 and 8024–8305 cal yr BP, respectively (median ages of 8380 and 8120 cal yr BP respectively; Table 1). By contrast, the age of the upper sand is poorly-constrained, with a single shell date collected from the silty clay 10 cm below the sand (Figure 2A) that has a median age of 7530 cal yr BP (Table 1). The site landowner, whose family have lived in Budle Bay since prior to 1870, described the abrupt transition from shell-bearing silty clay (unit 6, Figure 2A) to organic silty clay with sand inclusions (unit 5, Figure 2A), which occurs 1 cm above the dated sample in P2, as representing the building of a sea wall in 1870 CE. The presence of the sea wall caused tidal inundation of the coring sites to cease and the channel to dry up (Sutherland, 2018 *pers. comm.*). It is therefore likely that the upper sand is younger than 1870 CE, which would either mean the radiocarbon age (UBA-39041) is anomalously old, or there is a hiatus in

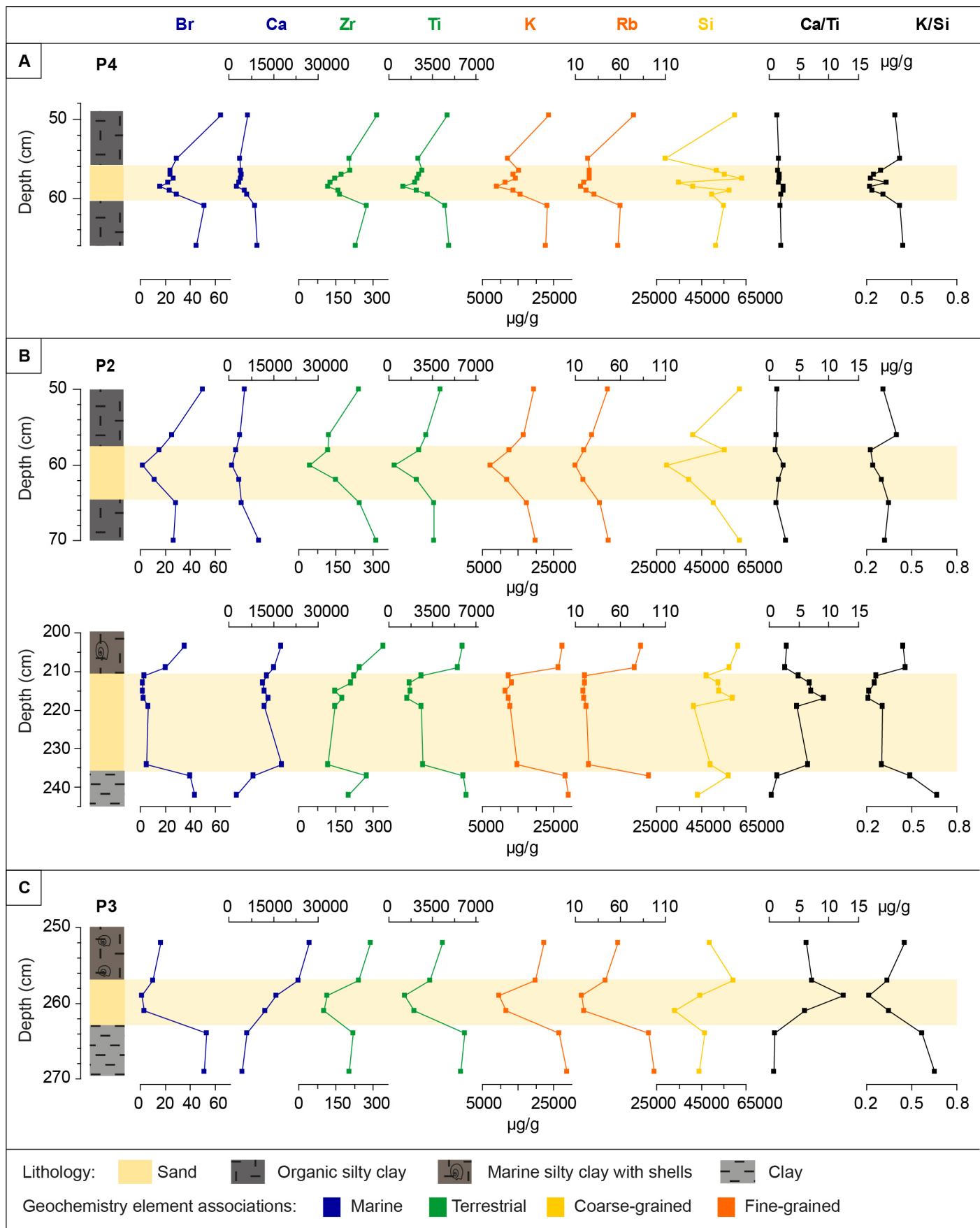


Figure 3 | Geochemical composition of the (A) upper sand in P4, (B) upper and lower sands in P2, and (C) lower sand in P3. The unit of measurement for all plots is $\mu\text{g/g}$.

sedimentation or erosion, potentially related to the building of the sea wall. Additional dating would be required to definitively confirm the age of the upper sand deposit.

4.5. Ground-penetrating radar profiles

Unfortunately, it was not possible to collect a GPR line over the coring sites due to the presence of water at the surface and the uneven topography, which was not able

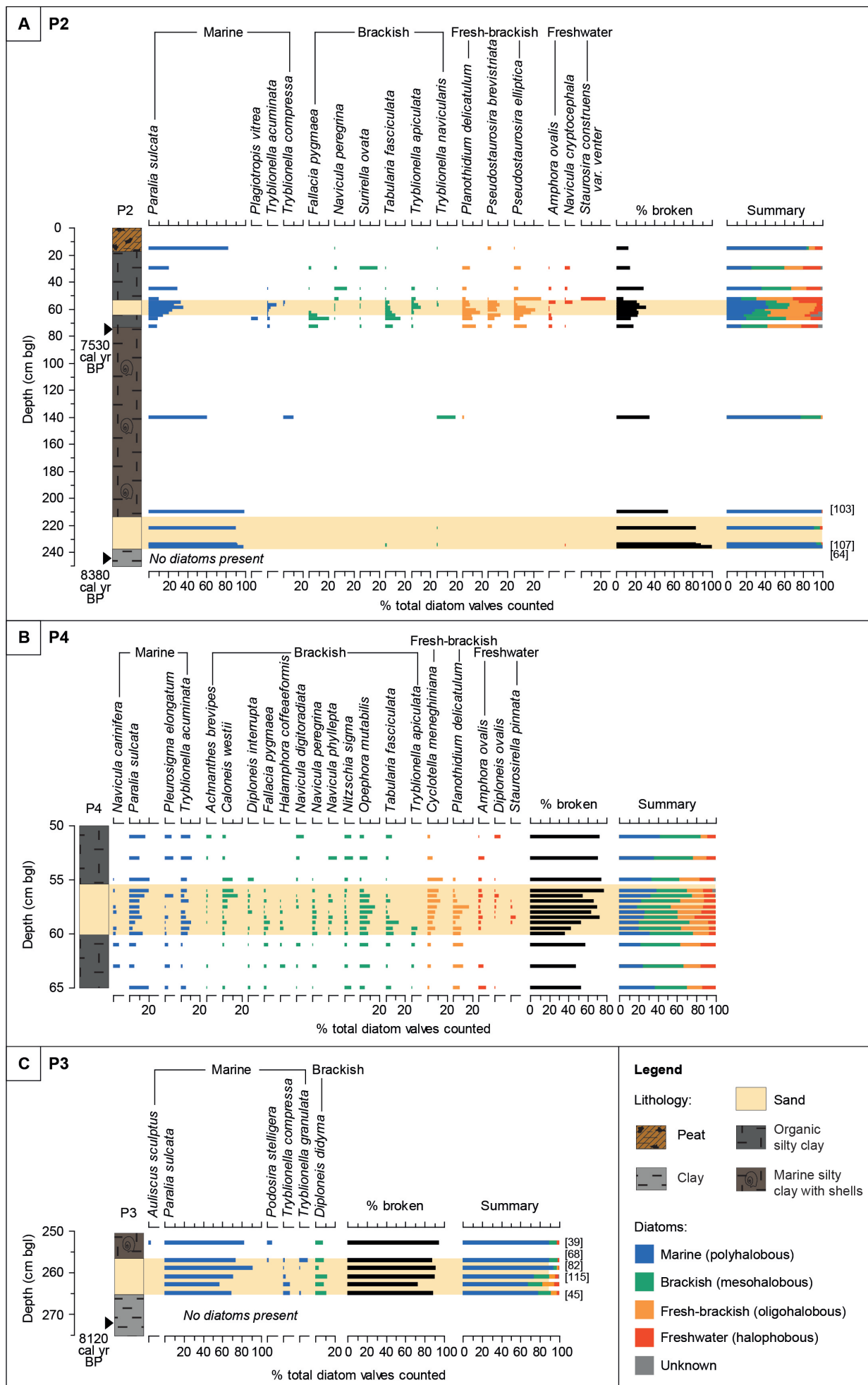


Figure 4 | Diatom assemblages of cores (A) P2, (B) P4 and (C) P3, showing species constituting >5% of any one sample. Where a minimum count of 250 valves could not be achieved from a sample, the total valves counted are indicated in brackets on the far right of the plot. Median calibrated radiocarbon ages are shown.

| Laboratory code | Core and sample depth (cm bgl) | Material dated | Radiocarbon age (yr BP $\pm 1\sigma$) | Calibrated age range with probability (2 σ cal yr BP) | Median calibrated age (cal yr BP) |
|-----------------|--------------------------------|----------------|--|---|-----------------------------------|
| UBA-39041 | P2 - 74 | Shell | 7239 \pm 27 | 7409 - 7657 (95.4%) | 7530 |
| UBA-39042 | P2 - 244 | Wood | 7570 \pm 49 | 8208 - 8261 (7.0%) 8305 - 8453 (88.0%) 8505 - 8512 (0.4%) | 8380 |
| UBA-39043 | P3 - 272 | Wood | 7344 \pm 40 | 8024 - 8210 (89.0%) 8261 - 8305 (6.5%) | 8120 |

Table 1 | Ages of samples from Budle Bay determined by AMS radiocarbon dating. The shell sample was calibrated in OxCal 4.4 (Bronk Ramsey, 2009) using the Marine20 calibration curve. Both wood samples were calibrated using the terrestrial IntCal20 calibration curve. The 2-sigma range of calibrated ages is reported, and median calibrated ages are rounded to the nearest 10 years.

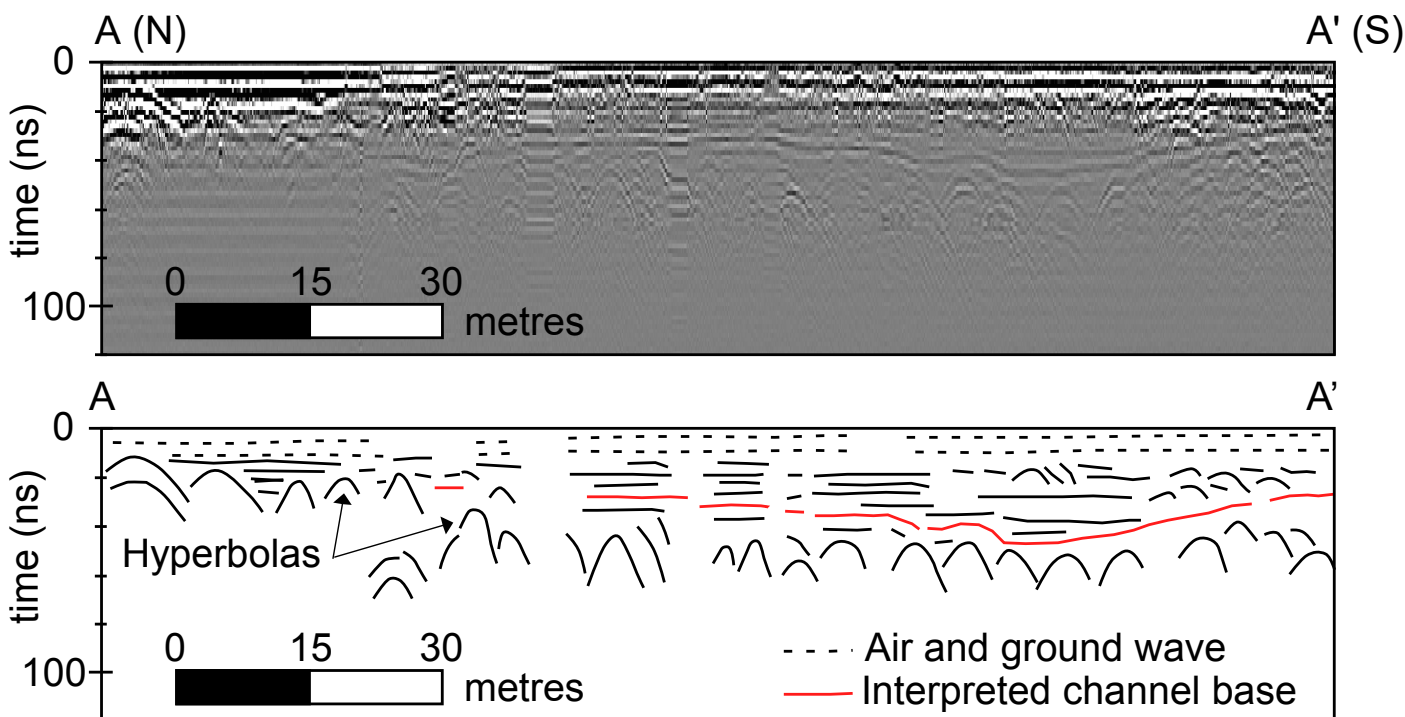


Figure 5 | Uninterpreted (top panel) and line interpretation (bottom panel) of GPR line 1.

to be corrected for (in the absence of a functioning GPS). In addition, given the thickness of the sand layer, the resolution of the GPR was likely too low for it to be detected. Nevertheless, the GPR lines do provide an opportunity to examine the deeper stratigraphy and overall geologic setting of the site.

All four GPR lines show a similar stratigraphy of a zone of hyperbolas at the base, overlain by continuous near parallel reflections onlapping the zone of hyperbolas, with some weakly-developed very shallow oblique reflections in the upper-most portions of the profiles (Figure 5). Assuming a radar velocity of 0.08 m/ns, the zone of hyperbolas was at depths of <1 m to ~3 m, with the weakly-developed oblique reflections all within the upper ~1.5 m. The upper continuous near-parallel reflections appear to fill a channel-like feature developed within the more southerly portions of the profile (Figure 5).

5. Discussion

The multi-proxy approach of this study follows previous successful studies aimed at distinguishing storm and tsunami deposits from surrounding low-energy deposits and

identifying the origins of tsunami deposits (e.g., Chagué-Goff et al., 2015; Nentwig et al., 2018; Gaffney et al., 2020). The benefit of a multi-proxy approach is in mitigating well-documented challenges associated with individual proxies such as post-depositional changes or poor micro-fossil preservation.

The combination of sedimentological, geochemical and diatom analyses suggests both sand units were deposited during high-energy marine incursion events. The evidence for this interpretation is discussed in the following sections, along with key evidence that helps to determine the depositional mechanism of the sands, and whether this varies between the sands.

5.1. Sedimentology

Deposition (or preservation) of sand beds is largely localised to the southwestern end of the palaeochannel, within the former lowland ponded area. The lower sand is not observed anywhere else, and the upper sand only observed in one other core in the palaeochannel. Given the absence of sand beds in cores from the same elevations (C1, C2, C4), we suggest that erosion within

the palaeochannel may have occurred. Whilst it is not possible to determine the origin of the sand bed on the basis of sedimentology alone, the sands display some features typical of deposition in tsunami or storms. Both the upper and lower sands, deposited between organic clays, have sharp lower contacts, suggesting deposition in a high-energy event. Particle size distributions of the two sands are different, with the lowermost being a fine- to medium-grained sand, and the base of the upper sand having a coarser grain size; essentially the deposit comprises a coarse-grained sand lens within a finer-grained sandy silt (Figure 2B). Whilst the sedimentology of the lower sand is consistent with Storegga deposits identified in the UK in terms of thickness, fine to medium grain size and being composed of a single fining upwards sequence (c.f. Dawson et al., 1988; Dawson & Smith, 2000; Smith et al., 2004), interpreting the origin of either sand bed on this basis alone is not possible, and instead evidence is sought from the geochemistry and diatom composition. Characteristic tsunami features such as rip-up clasts and flame structures were not observed; however, these are less likely to be identified in cores than in exposures or trenches.

5.2. Geochemistry

Principal component analysis (PCA) shows that the sand deposits have unique geochemical signatures, distinguishable from non-sand deposits on the basis of their geochemistry (Figure 6A). PCA also shows that the upper and lower sand deposits can be distinguished on the basis of their geochemical signatures. PC axis 1 accounts for 58% of the variance in the data, and is most strongly associated with Rb, K, and Ti, although it must be acknowledged that the variance explained by PC1 is relatively low. Sediment type appears to most strongly influence component 1, with sand samples displaying positive loadings along PC axis 1 and non-sands displaying negative loadings. The second PC axis accounts for only 22% of the variance in the data and is best explained by the presence of Ca (a marine indicator). Upper and lower sand samples plot discretely along axis 2, although the low amount of variance explained by PC2, means that this interpretation must be treated with caution.

Both the upper and lower sands are characterised by an increased marine signature (Ca/Ti), and a decline in elements indicative of terrestrial (Zr, Ti) and fine-grained material (K, Rb, and K/Si) compared to sediments above and below both sands. The decline of K and Rb is commonly witnessed in tsunami and storm studies (Cuven et al., 2013; Swindles et al., 2018) and is mainly associated with finer grained sediments, such as clays, which often surround the sands deposited by these events (Kylander et al., 2011; Ramírez-Herrera et al., 2012; Cuven et al., 2013; Chagué, 2020).

Increased concentrations of Ca/Ti throughout the sands support the interpretation of the sands being

marine-sourced. Whilst carbonates can form in terrestrial settings (e.g., palustrine carbonates, calcretes), Ca is well-correlated to marine indicators due to its dominance in marine biogenic or detrital carbonates (Chagué-Goff, 2010; Tsompanoglou et al., 2011; Cuven et al., 2013; Chagué-Goff et al., 2017; Swindles et al., 2018; Chagué, 2020; Gaffney et al., 2020). We make this interpretation with caution though, noting that further geochemical analysis would be required on potential local source material (e.g., beach and dune sand) that would have been entrained by the tsunami, to definitively confirm seaward provenance of sediment. Investigation of groundwaters would also be necessary, as at Budle Bay, Ca concentrations may reflect scouring of the underlying bedrock, which is composed of limestone strata of the Alston Formation (a calcium carbonate-rich formation), or equally may reflect marine or aeolian input, as beach and dune sands will very likely be derived of calcium carbonate also. One potential explanation for the difference in Ca concentrations between the upper and lower sands may be the composition of the two sand units in terms of grain size. The upper sand, whilst coarse at the very base, is predominantly sandy silt, and therefore likely contains a lower concentration of calcium carbonate mineral grains than compared with the lower sand.

Changes within the sand beds are also highlighted by declining concentrations of Br, Zr, and Ti (Figure 3). Br is often used as a saltwater indicator, but displays inverse trends to Ca within the lower sands (Figure 3). The low values do not necessarily rule out a marine source, as bromine is a water leachable ion, and therefore could have been leached from the sands into the surrounding sediment from subsequent rainfall (Chagué-Goff et al., 2017; Chagué, 2020). Bromine is known to have a strong affinity to finer grained organic-rich sediments (Biestler et al., 2004; Chagué-Goff, 2010; Chagué, 2020) and may explain why Br concentrations are greatest in the sediment surrounding the sand beds (Figure 3). Lower concentrations of Zr and Ti also highlight variations between the sediments. Zr and Ti can be associated with heavy minerals (Nichol et al., 2007; Ramírez-Herrera et al., 2012; Chagué-Goff et al., 2017), but are interpreted here as a reflection of terrestrial material (Gaffney et al., 2020), mimicking both K and Rb trends. The lower concentrations of terrestrial indicators in comparison to marine indicators supports the idea of a marine source for both sand beds.

5.3. Diatoms

Whilst the upper and lower sands are distinguishable on the basis of their geochemical signatures, diatom assemblages are harder to compare. PCA shows sand and non-sand samples cannot be distinguished solely on the basis of their diatom assemblages (Figure 6B), and whilst the upper and lower sand samples plot discretely along PC axis 2, the total amount of variance explained by PCs 1 and 2 is simply too low to be useful. This does, however,

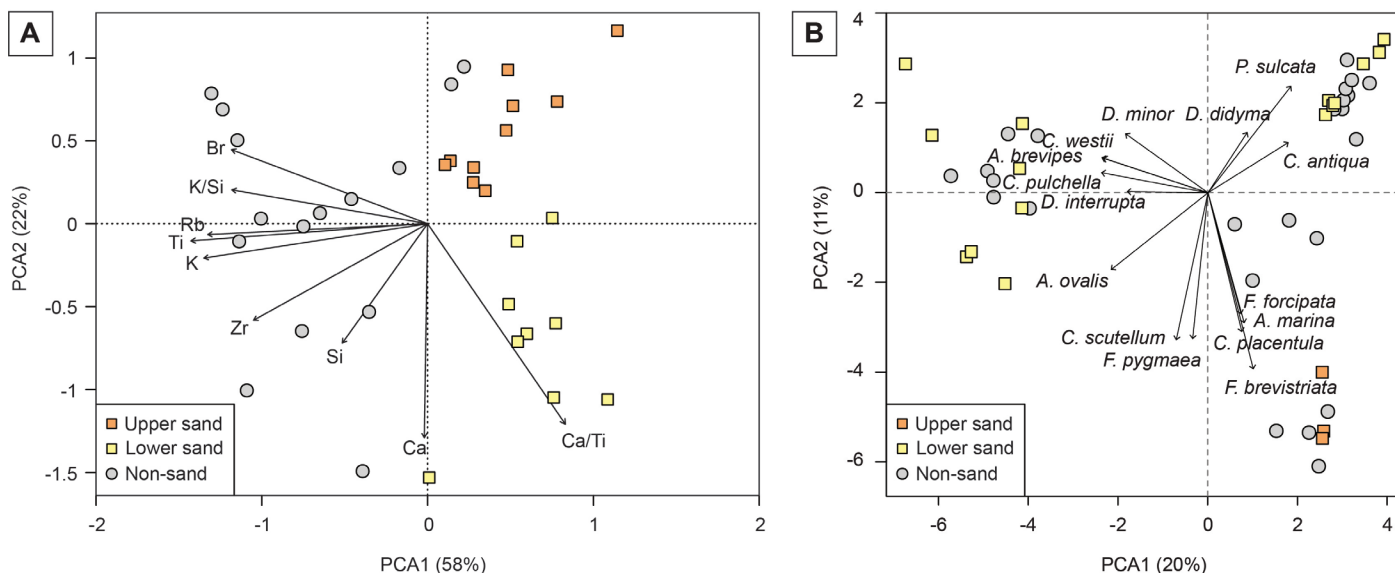


Figure 6 | Principal component analysis of (A) geochemical data from P4 and (B) diatom data from P2.

highlight the value of the geochemical data and multi-proxy approach.

The upper sand consists of mixed freshwater-brackish-marine diatom assemblages, which are similar to pre- and post-sand assemblages and contain relatively low percentages of broken valves (~14–30%). The similarity in assemblages and amounts of valve breakage between the upper sand and surrounding fine-grained deposits means it is not possible to infer the depositional mechanism of the upper sand on the basis of the diatoms alone. In contrast to the upper sand, the lowermost sand is characterised by marine taxa (*Paralia sulcata*) and a very high percentage of broken valves (sometimes up to 100% of the assemblage). High percentages (60–90%) of broken diatom valves are often associated with turbulent waves generated by tsunamis (Dawson et al., 1996; Dawson & Smith, 2000; Sawai et al., 2002; Dawson, 2007; Sawai et al., 2009; Dura & Hemphill-Haley, 2020). The lower sand contains few brackish and freshwater diatom species, something which is uncommon throughout tsunami and storm research. Typically, tsunamis and storms consist of chaotic diatom assemblages as they erode, transport, and redeposit marine, brackish, and freshwater taxa from diverse areas as they cross coastal and inland areas (Parsons, 1998; Cochran et al., 2005; Dawson, 2007; Morton et al., 2007; Nanayama et al., 2007; Sawai et al., 2009; Engel & Brückner, 2011; Dura & Hemphill-Haley, 2020; Hocking et al., 2021). The absence of a mixed diatom assemblage within the lower sands could be due to wave approach direction and current velocity (Sawai et al., 2009). At high flow speeds only benthic marine taxa, which attach to heavier sand, are able to settle out of the water column, which could explain the very low percentages of freshwater and brackish diatoms (Sawai et al., 2009). Alternatively, and perhaps a simpler explanation, however, is that the dominance of the sturdy valves of *Paralia sulcata*, as well as *Diploneis didyma*, may simply reflect the loss of other taxa to dissolution or winnowing within the lower sand deposit. Combined with the lower

overall diatom abundances in the lower sands, this may suggest a problem with diatom preservation in the lower sands rather than an actual difference in assemblage or sediment source between the upper and lower sands. The mixed diatom assemblage of the upper sand may be a result of better preservation in finer-grained sediment (sandy silt), as well as the core location in a former lowland ponded area. Therefore, whilst the diatom assemblage of the lower sand is consistent with Storegga deposits elsewhere in the UK, which are generally dominated by marine and brackish species, particularly *Paralia sulcata*, and high percentages of diatom valve breakage (Dawson et al., 1988; Dawson & Smith, 2000; Smith et al., 2004), it is not possible to link deposition of the lower sand deposit to the Storegga tsunami on the basis of the diatom assemblage alone, as this could equally be a function of diatom preservation rather than sediment source.

Deposition of the upper sand follows an abrupt change in diatom assemblage between units 6 (silty clay with shells) and 5 (silty clay). Whilst we acknowledge the gap in sampling through the top of the shelly clay, the diatom assemblage changes from 77% marine taxa at 140 cm to just 15% at 73 cm (the latter sample taken from immediately above the unit boundary; Figure 4A). Eyewitness accounts of local residents John Sutherland (2018 *pers. comm.*), whose family lived in Budle Bay in 1870) suggest the sharp transition from marine taxa to a mixed assemblage dominated by fresh and brackish taxa represents the construction of coastal defences in 1870 CE, which disconnected the area of the coring sites from the sea. Subsequently, the 1953 North Sea storm surge is known to have caused flooding of the Ross Peninsula (north shore of Budle Bay), with marine waters overtopping and damaging sea defences at Budle Bay (Guthrie et al., 2009). This event is a potential source for the deposition of the upper sand, and could explain the subsequent increase in marine diatoms within the uppermost sand. However, the timing cannot be corroborated by the radiocarbon date

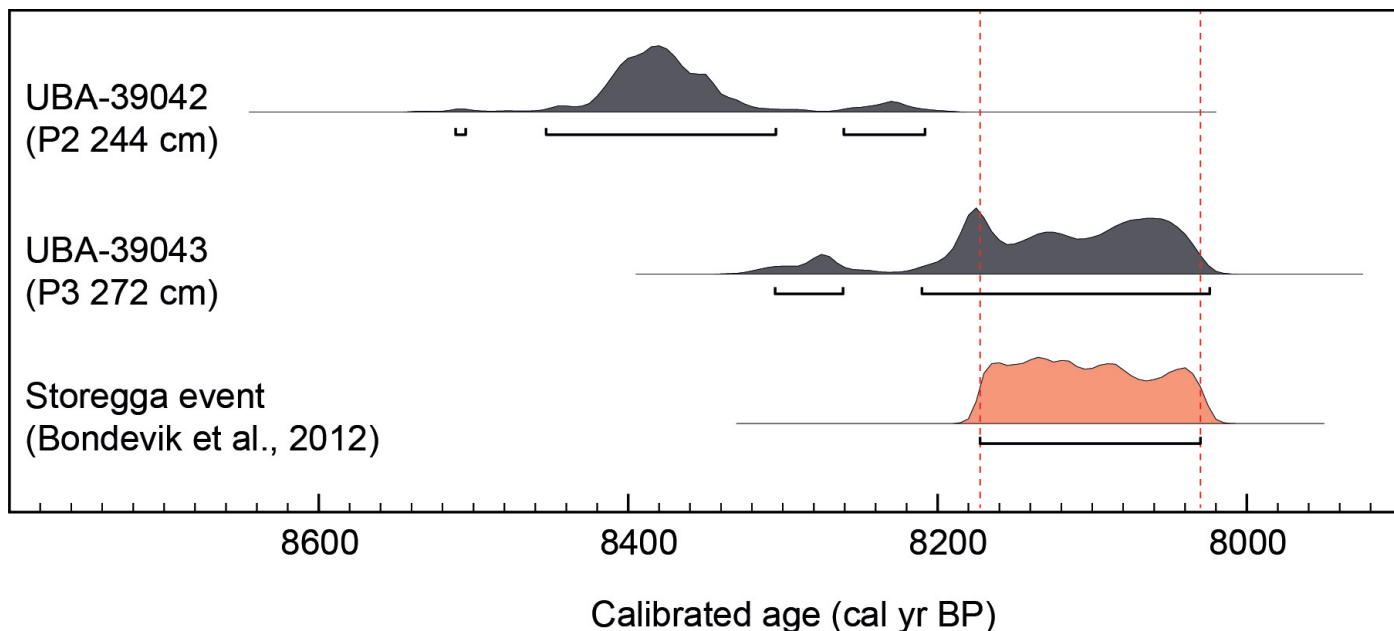


Figure 7 | Probability density functions for calibrated ages of samples below the lower sand layers in P2 and P3, which are compared to the age of the Storegga slide previously reported by Bondevik et al. (2012), and recalibrated here using IntCal20 in OxCal 4.4 (Bronk Ramsey, 2009; Reimer et al., 2020).

on the uppermost sand in this study, and additional age control would be required for confirmation.

5.4. Ground-penetrating radar interpretations

Although not directly connected to the core sites, the interpretation of the GPR profiles (Figure 5) provides an opportunity to examine the overall palaeogeographical setting of the site at the time of sand deposition. The basal hyperbolae are interpreted to represent either underlying till or bedrock. The overlying parallel reflections likely represent the finer-grained coastal plain muds sampled in the cores, with the weakly developed shallow oblique reflections likely representing the tidal and/or fluvial creeks observed beneath the footprint of the modern agriculture within aerial photographs (Figure 1E). The buried larger-scale channel-like feature, which appears to be incised into the till or bedrock (Figure 5), likely represents the fluvial drainage network flooded during the early Holocene sea-level rise before the highstand during the middle Holocene (Shennan et al., 2000). The roughly east-west trend of the channel imaged beneath the road in line 1 (Figure 1E) suggests it likely extends to the east, and may therefore represent a control upon the accommodation where the sands are preserved.

5.5. Implications of new evidence for the Storegga tsunami reaching Northumberland

The multi-proxy evidence provided here suggests that the lowermost sand may be tentatively attributed to the Storegga tsunami. Sedimentology and particle size distribution are consistent with a tsunami origin, with the lower sand consisting of fine- to medium-grained sand that fines upwards (Figure 2B). The diatoms support this interpretation, as they were predominantly fragmented, marine in origin, and dominated by *Paralia sulcata* (Figure

4), all of which are consistent with other Storegga tsunami deposits in the UK (Dawson et al., 1996; Dawson & Smith, 2000; Dawson, 2007). However, we do acknowledge that potential low diatom preservation in the lower sand may also explain the dominance of *Paralia sulcata* and prevent definitive correlation with the Storegga tsunami. Geochemical signatures are mixed, with increased concentrations of marine (Ca) and coarse-grained (Si) material in the lower sand compared to sediments above and below the sand (Figure 3). The greater concentration of marine elements in the lower sand compared to the uppermost sand may suggest a tsunami origin. However, erosion of the underlying bedrock and increased transport of terrestrial material (Gaffney et al., 2020), or an influx of Ca-rich beach or dune sand may also explain the higher elemental concentrations. Additional comparison with geochemical signatures of modern potential source material would be required to confirm the sediment source and depositional mechanism. Assuming that the lower sand beds in both P2 and P3 relate to the same event, radiocarbon ages place the timing of this event around 8120–8380 cal yr BP. This age coincides with previously reported ages of the Storegga tsunami of 8110 ± 100 cal yr BP (Dawson et al., 2011), 8070–8180 cal yr BP (Bondevik et al., 2012), and 8080–8180 cal yr BP (Rush et al., 2023) (Figure 7).

Evidence for Storegga tsunami inundation along other parts of the Northumberland coastline is inconclusive, with a possible correlative deposit at Broomhouse Farm (~10 km northeast of Budle Bay) recorded at a higher present-day elevation of 2.5–5.1 m OD (Shennan et al., 2000), compared to the lower sand at 0.4–0.9 m OD here. At Budle Bay, preservation of potential Storegga deposits appears to be localised and restricted to the pond location rather than across the entire site. It is possible that any deposits in the palaeochannel have subsequently been eroded. Therefore, whilst this study adds to the possible

evidence of Storegga Slide tsunami inundation reaching the Northumberland coastline (c.f. Shennan et al., 2000; Boomer et al., 2007), it also supports the suggestion that physical evidence for the Storegga tsunami is localised where conditions are favourable for preservation (Gaffney et al., 2020).

5.6. Limitations associated with the identification of tsunami deposits

Globally, challenges remain with trying to distinguish between tsunami and storm deposits, as they both show characteristics of marine inundation and leave similar traces within the stratigraphic record (Dawson, 1999; Dawson & Shi, 2000; Goff et al., 2004; Kortekaas & Dawson, 2007; Engel & Brückner, 2011; Pilarczyk et al., 2014; Dura et al., 2016; Engel et al., 2020). This challenge has been exacerbated by the small number of known locations where both types of deposits occur along the same stretch of coastline, meaning that site-specific variations such as geology, topography, and available source material cannot be considered (Kortekaas & Dawson, 2007). This absence of both deposits in the same setting has led to previous research being dominated by the study of one or the other deposit. Sedimentology and microfossils are key proxies used throughout tsunami and storm research (Dawson et al., 1996; Parsons, 1998; Dawson, 1999; Smith et al., 2004; Kortekaas & Dawson, 2007; Morton et al., 2007; Horton et al., 2009; Tsompanoglou et al., 2011; Pilarczyk et al., 2014; Goto et al., 2015; Swindles et al., 2018); however if applied in isolation here, these techniques and their results would have provided inconclusive origins of the uppermost sands, especially given their observed similarities to the lowermost sands.

Geochemistry has not been as widely applied in tsunami and storm research as other proxies (Chagué-Goff, 2010; Chagué, 2020), and our study highlights the issues that need to be addressed to fully realise the potential additional insights geochemical analyses can provide. Geochemical signatures can be altered due to post-depositional changes such as dilution and leaching due to rainfall, which cannot be easily quantified (Chagué et al., 2018). Geochemical signatures are also site-specific, meaning that not all elements indicative of tsunami and storms are preserved in each deposit. Knowledge of the underlying geology is critical for the interpretation of element concentrations. Despite these limitations, geochemistry provides useful critical additional information to supplement other proxies, and is recommended to be utilised amongst multi-proxy studies.

6. Conclusions

Sedimentological, geochemical, and microfossil datasets have been used in combination to investigate the origins of sand deposits at Budle Bay, Northumberland. The multi-proxy evidence provided here suggests that the lowermost sand may tentatively be attributed to the Storegga

tsunami event, and that the upper sand may relate to the 1953 North Sea storm surge. Additional chronological control, however, is required, particularly to support this latter interpretation. Both sands are characterised by elevated Ca/Ti and a decline in K/Si compared to non-sand sediments. However, the geochemical signatures differ between the upper and lower sands, particularly in terms of calcium concentrations. It is not possible from our analyses alone to determine whether this difference reflects differences in their sources (e.g., tsunami vs storm) or simply a difference in grain size between the two units. The potential issue of lower degrees of diatom preservation in the lower sand also means it is not possible to determine whether the dominance of a single marine taxon and a very high percentage of broken valves reflects a tsunami source, or simply the dissolution of less resistant taxa in coarser grained deposits.

Whilst we recognise that we are unable to provide conclusive evidence for the Storegga tsunami reaching Budle Bay, we do provide an additional potential occurrence of Storegga deposits alongside those previously proposed as potentially representing the Storegga tsunami in Northumberland. If the Storegga tsunami did reach Budle Bay, this would be the most southerly onshore site within the United Kingdom to contain the deposit. The inconclusive evidence, however, critically affirms the localised nature of preservation of the Storegga tsunami. The challenges involved in differentiating depositional mechanisms only serve to highlight the necessity of a multi-proxy approach. We also emphasise the importance of considering local geology and post-depositional changes when interpreting geochemical data. Used in combination, sedimentology, geochemistry and micropalaeontology provide a useful toolkit for the identification of tsunami deposits and their differentiation from storm deposits.

Acknowledgments

We gratefully acknowledge John Sutherland for allowing site access and providing eyewitness accounts and historical context. We kindly thank the Quaternary Research Association for the QRA-14CHRONO Centre Radiocarbon Dating Award (2018 to LP), as well as Prof. Reimer and Mr Stephen Hoper for their assistance with radiocarbon dating. We also thank Drs. Matthew Pound, James Walker, Sophie Williams and Luke Andrews for their help on fieldwork, and Prof. Jeff Warburton for help with processing GPR data. AS was supported by the US-UK Fulbright Commission. We kindly thank two anonymous reviewers for their comments, which greatly improved the manuscript. All maps were created using ArcGIS Pro® software version 3.1.3 by Esri. ArcGIS® and ArcGIS Pro™ are the intellectual property of Esri and are used herein under license. Copyright © Esri. All rights reserved.

Authors contribution

EH, LP, GS conceived the initial research project; LP, EH, EG, AS conducted the fieldwork; LP, GS, EH conducted the diatom analysis; GS conducted the geochemical analysis; EG, AS conducted the GPR survey; all authors wrote and contributed to the manuscript.

Data availability

Diatom, geochemistry, and particle size data sets are available on the Figshare repository: <https://doi.org/10.6084/m9.figshare.24260632.v2>

Conflict of interest

The authors declare no competing interests.

References

- Battarbee, R.W. (1986). Diatom analysis. In: Berglund, B.E. (Ed.) *Handbook of Holocene Palaeoecology and Palaeohydrology*. John Wiley, pp. 527-557. <https://doi.org/10.1002/jqs.3390010111>
- Battarbee, R.W., Carvalho, L., Jones, V.J., Flower, R.J., Cameron, N.G., Bennion, H. & Juggins, S. (2001). Diatoms. In: Smol, J.P., Birks, H.J.B. & Last, W.M. (Eds.) *Tracking Environmental Change Using Lake Sediments. Volume 3: Terrestrial, Algal, and Siliceous Indicators*. Kluwer, pp. 155-202. https://doi.org/10.1007/0-306-47668-1_8
- Biester, H., Keppler, F., Putschew, A., Martinez-Cortizas, A. & Petri, M. (2004). Halogen retention, organohalogens, and the role of organic matter decomposition on halogen enrichment in two Chilean peat bogs. *Environmental Science & Technology*, 38(7), 1984-1991. <https://doi.org/10.1021/es0348492>
- Bondevik, S., Løvholth, F., Harbitz, C., Mangerud, J., Dawson, A. & Svendsen, J.I. (2005). The Storegga Slide tsunami - comparing field observations with numerical simulations. In: Solheim, A., Bryn, P., Berg, K., Sejrup, H.P., Mienert, J. (Eds.) *Ormen Lange – an Integrated Study for Safe Field Development in the Storegga Submarine Area*. Elsevier, pp. 195-208. <https://doi.org/10.1016/B978-0-08-044694-3.50021-4>
- Bondevik, S., Mangerud, J., Dawson, S., Dawson, A. & Lohne, Ø. (2003). Record-breaking height for 8000-year old tsunami in the North Atlantic. *Eos*, 84(31), 289-300. <https://doi.org/10.1029/2003EO310001>
- Bondevik, S., Stormo, S.K. & Skjerdal, G. (2012). Green mosses date the Storegga tsunami to the chilliest decades of the 8.2 ka cold event. *Quaternary Science Reviews*, 45, 1-6. <https://doi.org/10.1016/j.quascirev.2012.04.020>
- Bondevik, S., Svendsen, J.I. & Mangerud, J. (1997). Tsunami sedimentary facies deposited by the Storegga tsunami in shallow marine basins and coastal lakes, western Norway. *Sedimentology*, 44(6), 1115-1131. <https://doi.org/10.1046/j.1365-3091.1997.d01-63.x>
- Boomer, I., Waddington, C., Stevenson, T. & Hamilton, D. (2007). Holocene coastal change and geoarchaeology at Howick, Northumberland, UK. *The Holocene*, 17(1), 89-104. <https://doi.org/10.1177/0959683607073281>
- British Geological Survey (2020). *GeolIndex Onshore*, 1:50,000. <https://www.bgs.ac.uk/map-viewers/geoindex-onshore/>
- Bronk Ramsey, C. (2009) Bayesian analysis of radiocarbon dates. *Radiocarbon*, 51(1), 337-360. <https://doi.org/10.1017/S0033822200033865>
- Chagué, C. (2020). Applications of geochemical proxies in paleotsunami research. In: Engel, M., Pilarczyk, J., May, S.M., Brill, D., Garrett, E. (Eds.) *Geological Records of Tsunamis and Other Extreme Waves*. Elsevier, pp. 381-401. <https://doi.org/10.1016/B978-0-12-815686-5.00018-3>
- Chagué, C., Sugawara, D., Goto, K., Goff, J., Dudley, W. & Gadd, P. (2018). Geological evidence and sediment transport modelling for the 1946 and 1960 tsunamis in Shinmachi, Hilo, Hawaii. *Sedimentary Geology*, 364, 319-333. <https://doi.org/10.1016/j.sedgeo.2017.09.010>
- Chagué-Goff, C. (2010). Chemical signatures of palaeotsunamis: a forgotten proxy? *Marine Geology*, 271(1-2), 67-71. <https://doi.org/10.1016/j.margeo.2010.01.010>
- Chagué-Goff, C., Goff, J., Wong, H.K.Y. & Cisternas, M. (2015) Insights from geochemistry and diatoms to characterise a tsunami's deposit and maximum inundation limit. *Marine Geology*, 359, 22-34. <https://doi.org/10.1016/j.margeo.2014.11.009>
- Chagué-Goff, C., Szczuciński, W. & Shinozaki, T. (2017). Applications of geochemistry in tsunami research: A review. *Earth-Science Reviews*, 165, 203-244. <https://doi.org/10.1016/j.earscirev.2016.12.003>
- Cochran, U.A., Berryman, K.R., Mildenhall, D.C., Hayward, B.W., Southall, K. & Hollis, C.J. (2005). Towards a record of Holocene tsunami and storms for northern Hawke's Bay, New Zealand. *New Zealand Journal of Geology and Geophysics*, 48(3), 507-515. <https://doi.org/10.1080/00288306.2005.9515129>
- Cuven, S., Paris, R., Falvard, S., Miot-Noirault, E., Benbakkar, M., Schneider, J.L. & Billy, I. (2013). High-resolution analysis of a tsunami deposit: Case-study from the 1755 Lisbon tsunami in southwestern Spain. *Marine Geology*, 337, 98-111. <https://doi.org/10.1016/j.margeo.2013.02.002>
- Davidson, N.C. & Buck, A.L. (1997). *An inventory of UK estuaries. Volume 1 Introduction and methodology*. Joint Nature Conservation Committee.
- Dawson, A.G. (1999). Linking tsunami deposits, submarine slides and offshore earthquakes. *Quaternary International*, 60(1), 119-126. [https://doi.org/10.1016/S1040-6182\(99\)00011-7](https://doi.org/10.1016/S1040-6182(99)00011-7)
- Dawson, A., Bondevik, S. & Teller, J.T. (2011). Relative timing of the Storegga submarine slide, methane release, and climate change during the 8.2ka cold event. *The Holocene*, 21(7), 1167-1171. <https://doi.org/10.1177/0959683611400467>
- Dawson, A.G., Long, D. & Smith, D.E. (1988). The Storegga slides: evidence from eastern Scotland for a possible tsunami. *Marine Geology*, 82(3-4), 271-276. [https://doi.org/10.1016/0025-3227\(88\)90146-6](https://doi.org/10.1016/0025-3227(88)90146-6)
- Dawson, A.G. & Shi, S. (2000). Tsunami deposits. *Pure and Applied Geophysics*, 157, 875-897. <https://doi.org/10.1007/s000240050010>
- Dawson, S. (2007). Diatom biostratigraphy of tsunami deposits: examples from the 1998 Papua New Guinea tsunami. *Sedimentary Geology*, 200(3-4), 328-335. <https://doi.org/10.1016/j.sedgeo.2007.01.011>
- Dawson, S. & Smith, D.E. (2000). The sedimentology of Middle Holocene tsunami facies in northern Sutherland, Scotland, UK. *Marine Geology*, 170(1-2), 69-79. [https://doi.org/10.1016/S0025-3227\(00\)00066-9](https://doi.org/10.1016/S0025-3227(00)00066-9)
- Dawson, S., Smith, D.E., Ruffman, A. & Shi, S. (1996). The diatom biostratigraphy of tsunami sediments: examples from recent and middle Holocene events. *Physics and*

- Chemistry of the Earth, 21(1-2), 87-92. [https://doi.org/10.1016/S0079-1946\(97\)00015-3](https://doi.org/10.1016/S0079-1946(97)00015-3)
- Dura, T., Hemphill-Haley, E., Sawai, Y. & Horton, B.P. (2016). The application of diatoms to reconstruct the history of subduction zone earthquakes and tsunamis. *Earth-Science Reviews*, 152, 181-197. <https://doi.org/10.1016/j.earscirev.2015.11.017>
- Dura, T. & Hemphill-Haley, E. (2020). Diatoms in tsunami deposits. In: Engel, M., Pilarczyk, J., May, S.M., Brill, D., Garrett, E. (Eds.) *Geological Records of Tsunamis and Other Extreme Waves*. Elsevier, pp. 291-322. <https://doi.org/10.1016/B978-0-12-815686-5.00014-6>
- Engel, M. & Brückner, H. (2011). The identification of palaeo-tsunami deposits – a major challenge in coastal sedimentary research. *Coastline Reports*, 17, 65-80.
- Engel, M., Pilarczyk, J., May, S.M., Brill, D. & Garrett, E. (2020). *Geological Records of Tsunamis and Other Extreme Waves*. Elsevier. <https://doi.org/10.1016/C2017-0-03458-4>
- Fruergaard, M., Piasecki, S., Johannessen, P.N., Noe-Nygaard, N., Andersen, T.J., Pejrup, M. & Nielsen, L.H. (2015). Tsunami propagation over a wide, shallow continental shelf caused by the Storegga slide, southeastern North Sea, Denmark. *Geology*, 43(12), 1047-1050. <https://doi.org/10.1130/G37151.1>
- Gaffney, V., Fitch, S., Bates, M., Ware, R.L., Kinnaird, T., Gearey, B., Hill, T., Telford, R., Batt, C., Stern, B., Whittaker, J., Davies, S., Ben Sharada, M., Everett, R., Cribdon, R., Kistler, L., Harris, S., Kearney, K., Walker, J., Muru, M., Hamilton, D., Law, M., Finlay, A., Bates, R. & Allaby, R.G. (2020). Multi-proxy characterisation of the Storegga tsunami and its impact on the early Holocene landscapes of the southern North Sea. *Geosciences*, 10(7), 270. <https://doi.org/10.3390/geosciences10070270>
- Goff, J., McFadgen, B.G. & Chagué-Goff, C. (2004). Sedimentary differences between the 2002 Easter storm and the 15th-century Okoropunga tsunami, southeastern North Island, New Zealand. *Marine Geology*, 204(1-2), 235-250. [https://doi.org/10.1016/S0025-3227\(03\)00352-9](https://doi.org/10.1016/S0025-3227(03)00352-9)
- Google Earth (2019) Budle Bay 55°37'01.36"N, 1°46'57.63"W [Online] Available at: <http://www.google.com/earth/index.html>
- Goto, T., Satake, K., Sugai, T., Ishibe, T., Harada, T. & Murotani, S. (2015) Historical tsunami and storm deposits during the last five centuries on the Sanriku coast, Japan. *Marine Geology*, 367, 105-117. <https://doi.org/10.1016/j.margeo.2015.05.009>
- Grauert, M., Björck, S. & Bondevik, S. (2001). Storegga tsunami deposits in a coastal lake on Suduroy, the Faroe Islands. *Boreas*, 30(4), 263-271. <https://doi.org/10.1111/j.1502-3885.2001.tb01045.x>
- Guthrie, G., Cooper, N., Howell, D., Cooper, T., Gardiner, J., Lawton, P., Gregory, A. & Stevens, R. (2009). Northumberland and North Tyneside Shoreline Management Plan 2. Royal Haskoning.
- Hafliðason, H., Lien, R., Sejrup, H.P., Forsberg, C.F. & Bryn, P. (2005). The dating and morphometry of the Storegga Slide. *Marine and Petroleum Geology*, 22(1-2) 123-136. <https://doi.org/10.1016/j.marpetgeo.2004.10.008>
- Hartley, B. (1996) *An Atlas of British Diatoms*. Biopress.
- Heaton, T.J., Köhler, P., Butzin, M., Bard, E., Reimer, R.W., Austin, W.E.N., Bronk Ramsey, C., Grootes, P.M., Hughen, K.A., Kromer, B., Reimer, P.J., Adkins, J., Burke, A., Cook, M.S., Olsen, J. & Skinner, L.C. (2020). Marine20 - The marine radiocarbon age calibration curve (0-55,000 cal BP). *Radiocarbon*, 62(4), 779-820. <https://doi.org/10.1017/RDC.2020.68>
- Hocking, E.P., Garrett, E., Aedo, D., Carvajal, M. & Melnick, D. (2021). Geological evidence of an unreported historical Chilean tsunami reveals more frequent inundation. *Communications Earth and Environment*, 2, 245. <https://doi.org/10.1038/s43247-021-00319-z>
- Horton, B.P., Rossi, V. & Hawkes, A.D. (2009). The sedimentary record of the 2005 hurricane season from the Mississippi and Alabama coastlines. *Quaternary International*, 195(1-2), 15-30. <https://doi.org/10.1016/j.quaint.2008.03.004>
- Jüttner, I., Carter, C., Chudaev, D., Cox, E.J., Ector, L., Jones, V., Kelly, M.G., Kennedy, B., Mann, D.G., Turner, J.A., Van de Vijver, B., Wetzel, C.E. & Williams, D.M. (2023). *Freshwater Diatom Flora of Britain and Ireland Amgueddfa Cymru - National Museum of Wales*. <https://naturalhistory.museumwales.ac.uk/diatoms>
- Kortekaas, S. & Dawson, A.G. (2007). Distinguishing tsunami and storm deposits: an example from Martinhal, SW Portugal. *Sedimentary Geology*, 200(3-4), 208-221. <https://doi.org/10.1016/j.sedgeo.2007.01.004>
- Kylander, M.E., Ampel, L., Wohlfarth, B. & Veres, D. (2011). High-resolution X-ray fluorescence core scanning analysis of Les Echets (France) sedimentary sequence: new insights from chemical proxies. *Journal of Quaternary Science*, 26(1), 109-117. <https://doi.org/10.1002/jqs.1438>
- Leynaud, D., Mienert, J. & Vanneste, M. (2009). Submarine mass movements on glaciated and non-glaciated European continental margins: A review of triggering mechanisms and preconditions to failure. *Marine and Petroleum Geology*, 26(5), 618-632. <https://doi.org/10.1016/j.marpetgeo.2008.02.008>
- Linsley, S. (2005). *Ports and Harbours of Northumberland*. Tempus Publishing.
- Long, A.J., Barlow, N.L.M., Dawson, S., Hill, J., Innes, J.B., Kelham, C., Milne, F.D. & Dawson, A. (2016). Lateglacial and Holocene relative sea-level changes and first evidence for the Storegga tsunami in Sutherland, Scotland. *Journal of Quaternary Science*, 31(3), 239-255. <https://doi.org/10.1002/jqs.2862>
- Micallef, A., Masson, D.G., Berndt, C. & Stow, D.A.V. (2009). Development and mass movement processes of the north-eastern Storegga Slide. *Quaternary Science Reviews*, 28(5-6), 433-448. <https://doi.org/10.1016/j.quascirev.2008.09.026>
- Morton, R.A., Gelfenbaum, G. & Jaffe, B.E. (2007). Physical criteria for distinguishing sandy tsunami and storm deposits using modern examples. *Sedimentary Geology*, 200(3-4), 184-207. <https://doi.org/10.1016/j.sedgeo.2007.01.003>
- Nanayama, F., Furukawa, R., Shigeno, K., Makino, A., Soeda, Y. & Igarashi, Y. (2007). Nine unusually large tsunami deposits from the past 4000 years at Kiritappu marsh along the southern Kuril Trench. *Sedimentary Geology*, 200(3-4), 275-294. <https://doi.org/10.1016/j.sedgeo.2007.01.008>
- Nentwig, V., Bahlburg, H., Górecka, E., Huber, B., Bellanova, P., Witkowski, A. & Encinas, A. (2018). Multiproxy analysis of tsunami deposits - The Tirúa example, central Chile. *Geosphere*, 14(3), 1067-1086. <https://doi.org/10.1130/GES01528.1>
- Nichol, S.L., Goff, J.R., Devoy, R.J.N., Chagué-Goff, C., Hayward, B. & James, I. (2007). Lagoon subsidence and tsunami on the West Coast of New Zealand. *Sedimentary Geology*, 200(3-4), 248-262. <https://doi.org/10.1016/j.sedgeo.2007.01.019>
- Parsons, M.L. (1998). Salt marsh sedimentary record of the landfall of Hurricane Andrew on the Louisiana coast: diatoms and other paleoindicators. *Journal of Coastal Research*, 14(3), 939-950.

- Pilarczyk, J.E., Dura, T., Horton, B.P., Engelhart, S.E., Kemp, A.C. & Sawai, Y. (2014). Microfossils from coastal environments as indicators of paleo-earthquakes, tsunamis and storms. *Palaeogeography, Palaeoclimatology, Palaeoecology*, 413, 144-157. <https://doi.org/10.1016/j.palaeo.2014.06.033>
- Ramírez-Herrera, M.T., Lagos, M., Hutchinson, I., Kostoglodov, V., Machain, M.L., Caballero, M., Goguitchaichvili, A., Aguilar, B., Chagué-Goff, C., Goff, J., Ruiz-Fernández, A.C., Ortiz, M., Nava, H., Bautista, F., Lopez, G.I. & Quintana, P. (2012). Extreme wave deposits on the Pacific coast of Mexico: Tsunamis or storms? — A multi-proxy approach. *Geomorphology*, 139-140, 360-371. <https://doi.org/10.1016/j.geomorph.2011.11.002>
- Reimer, P.J., Austin, W.E.N., Bard, E., Bayliss, A., Blackwell, P.G., Bronk Ramsey, C., Butzin, M., Cheng, H., Edwards, R.L., Friedrich, M., Grootes, P.M., Guilderson, T.P., Hajdas, I., Heaton, T.J., Hogg, A.G., Hughen, K.A., Kromer, B., Manning, S.W., Muscheler, R., Palmer, J.G., Pearson, C., van der Plicht, J., Reimer, R.W., Richards, D.A., Scott, E.M., Southon, J.R., Turney, C.S.M., Wacker, L., Adolphi, F., Büntgen, U., Capano, M., Fahrni, S.M., Fogtmann-Schulz, A., Friedrich, R., Köhler, P., Kudsk, S., Miyake, F., Olsen, J., Reinig, F., Sakamoto, M., Sookdeo, A. & Talamo, S. (2020). The IntCal20 Northern Hemisphere radiocarbon age calibration curve (0-55 cal kBP). *Radiocarbon*, 62(4), 725-757. <https://doi.org/10.1017/RDC.2020.41>
- Rush, G., Garrett, E., Bateman, M.D., Bigg, G.R., Hibbert, F.D., Smith, D.E. & Gehrels, W.R. (2023). The magnitude and source of meltwater forcing of the 8.2 ka climate event constrained by relative sea-level data from eastern Scotland. *Quaternary Science Advances*, 100119. <https://doi.org/10.1016/j.qsa.2023.100119>
- Russell, N., Cook, G.T., Ascough, P.L. & Scott, E.M. (2015). A period of calm in Scottish seas: A comprehensive study of ΔR values for the northern British Isles coast and the consequent implications for archaeology and oceanography. *Quaternary Geochronology*, 30, 34-41. <https://doi.org/10.1016/j.quageo.2015.08.001>
- Sawai, Y., Jankaew, K., Martin, M.E., Prendergast, A., Choowong, M. & Charoentitirat, T. (2009). Diatom assemblages in tsunami deposits associated with the 2004 Indian Ocean tsunami at Phra Thong Island, Thailand. *Marine Micropaleontology*, 73(1-2), 70-79. <https://doi.org/10.1016/j.marmicro.2009.07.003>
- Sawai, Y., Nasu, H. & Yasuda, Y. (2002). Fluctuations in relative sea-level during the past 3000 yr in the Onnetoh estuary, Hokkaido, northern Japan. *Journal of Quaternary Science*, 17(5-6), 607-622. <https://doi.org/10.1002/jqs.708>
- Sharrocks, P.D. & Hill, J. (2023) Evaluating the impact of the Storegga tsunami on Mesolithic communities in Northumberland. *Journal of Quaternary Science*. <https://doi.org/10.1002/jqs.3586>
- Shennan, I., Horton, B., Innes, J., Gehrels, R., Lloyd, J., McArthur, J. & Rutherford, M. (2000). Late Quaternary sea-level changes, crustal movements and coastal evolution in Northumberland, UK. *Journal of Quaternary Science*, 15(3), 215-237. [https://doi.org/10.1002/\(SICI\)1099-1417\(200003\)15:3%3C215::AID-JQS505%3E3.0.CO;2-%23](https://doi.org/10.1002/(SICI)1099-1417(200003)15:3%3C215::AID-JQS505%3E3.0.CO;2-%23)
- Smith, D.E., Shi, S., Cullingford, R.A., Dawson, A.G., Dawson, S., Firth, C.R., Foster, I.D.L., Fretwell, P.T., Haggart, B.A., Holloway, L.K. & Long, D. (2004). The Holocene Storegga slide tsunami in the United Kingdom. *Quaternary Science Reviews*, 23(23-24), 2291-2321. <https://doi.org/10.1016/j.quascirev.2004.04.001>
- Sutherland, J. (2018 pers. comm.) Personal communication: conversation on 26th June 2018 at Ross Farm, Budle Bay.
- Swindles, G.T., Galloway, J.M., Macumber, A.L., Croudace, I.W., Emery, A.R., Woulds, C., Bateman, M.D., Parry, L., Jones, J.M., Selby, K., Rushby, G.T., Baird, A.J., Woodroffe, S.A. & Barlow, N.L.M. (2018). Sedimentary records of coastal storm surges: Evidence of the 1953 North Sea event. *Marine Geology*, 403, 262-270. <https://doi.org/10.1016/j.margeo.2018.06.013>
- Tappin, D.R. (2017). Tsunamis from submarine landslides. *Geology Today*, 33(5), 190-200. <https://doi.org/10.1111/gto.12200>
- Troels-Smith, J. (1955). Karakterisering af løse jordarter (Characterisation of unconsolidated sediments). *Danmarks Geologiske Undersøgelse IV. Række*, 3(10), 1-73. <https://doi.org/10.34194/raekke4.v3.6989>
- Tsompanoglou, K., Croudace, I.W., Birch, H. & Collins, M. (2011). Geochemical and radiochronological evidence of North Sea storm surges in salt marsh cores from The Wash embayment (UK). *The Holocene*, 21(2), 225-236. <https://doi.org/10.1177/0959683610378878>
- Wagner, B., Bennike, O., Klug, M. & Cremer, H. (2007). First identification of Storegga tsunami deposits from East Greenland. *Journal of Quaternary Science*, 22(4) 321-325. <https://doi.org/10.1002/jqs.1064>
- Wilson, P., Orford, J.D., Knight, J., Braley, S.M. & Wintle, A.G. (2001). Late Holocene (post-4000 years BP) coastal dune development in Northumberland, northeast England. *The Holocene*, 11(2), 215-229. <https://doi.org/10.1191/095968301667179797>
- Woodroffe, S.A., Hill, J., Bustamante-Fernandez, E., Lloyd, J.M., Luff, J., Richards, S. & Shennan, I. (2023). On the varied impact of the Storegga tsunami in northwest Scotland. *Journal of Quaternary Science*. <https://doi.org/10.1002/jqs.3539>

How to cite: Pickering, L. O., Summers, G. F., Hocking, E. P., Garrett, E., & Simms, A. R. (2024). Microfossil and geochemical evidence for the Storegga tsunami at Budle Bay, Northumberland, UK. *Sedimentologica*, 2(2), 1-15. <https://doi.org/10.57035/journals/sdk.2024.e22.1280>

